

Fully motorized optical-resolution photoacoustic microscopy

Lei Li,^{1,2} Chenghung Yeh,^{1,2} Song Hu,^{2,3} Lidai Wang,² Brian T. Soetikno,² Ruimin Chen,⁴ Qifa Zhou,⁴ K. Kirk Shung,⁴ Konstantin I. Maslov,² and Lihong V. Wang^{1,2,*}

¹Department of Electrical and System Engineering, Washington University in St. Louis One Brookings Dr., St. Louis, Missouri 63130, USA

²Optical Imaging Laboratory, Department of Biomedical Engineering, Washington University in St. Louis, One Brookings Dr., St. Louis, Missouri 63130, USA

³Department of Biomedical Engineering, University of Virginia, P.O. Box 800759, Charlottesville, Virginia 22908, USA

⁴Resource Center for Medical Ultrasonic Transducer Technology, Department of Biomedical Engineering, University of Southern California, 1042 Downey Way, DRB 136, Los Angeles, California 90089-1111, USA

*Corresponding author: lhwang@wustl.edu

Received December 11, 2013; accepted February 8, 2014;
posted March 3, 2014 (Doc. ID 202913); published March 28, 2014

We have developed fully motorized optical-resolution photoacoustic microscopy (OR-PAM), which integrates five complementary scanning modes and simultaneously provides a high imaging speed and a wide field of view (FOV) with 2.6 μm lateral resolution. With one-dimensional (1D) motion-mode mechanical scanning, we measured the blood flow through a cross section of a blood vessel *in vivo*. With two-dimensional (2D) optical scanning at a laser repetition rate of 40 kHz, we achieved a 2 kHz B-scan rate over a range of 50 μm with 20 A-lines and 50 Hz volumetric-scan rate over a FOV of 50 μm \times 50 μm with 400 A-lines, which enabled real-time tracking of cellular dynamics *in vivo*. With synchronized 1D optical and 2D mechanical hybrid scanning, we imaged a 10 mm \times 8 mm FOV within three minutes, which is 20 times faster than the conventional mechanical scan in our second-generation OR-PAM. With three-dimensional mechanical contour scanning, we maintained the optimal signal-to-noise ratio and spatial resolution of OR-PAM while imaging objects with uneven surfaces, which is essential for quantitative studies. © 2014 Optical Society of America

OCIS codes: (170.3880) Medical and biological imaging; (170.5120) Photoacoustic imaging; (180.5810) Scanning microscopy; (180.6900) Three-dimensional microscopy.

<http://dx.doi.org/10.1364/OL.39.002117>

Optical-resolution photoacoustic microscopy (OR-PAM), based on the photoacoustic effect [1], detects optical absorption contrasts with greater sensitivity than all other optical imaging modalities [2]. The high detection efficiency of intrinsic optical absorbers (e.g., oxy-hemoglobin (HbO₂) and deoxy-hemoglobin (HbR) [3,4]) enables OR-PAM to provide label-free, high-resolution [5,6], functional imaging of fine structures [7]. OR-PAM has already demonstrated broad biomedical applications in the fields of neurology [8], ophthalmology [9–12], and vascular biology [13]. However, the imaging speed of second-generation (G2) OR-PAM is insufficient for tracking certain fast dynamic activities *in vivo* [14]. Here, we report a fully motorized OR-PAM (FM-OR-PAM), which provides five scanning modes with fast imaging speed and a wide field of view (FOV).

The FM-OR-PAM system (Fig. 1) employs a wavelength-tunable laser system (INNOSLAB, Edgewave BX2II-E) for photoacoustic irradiation. The output laser beam (7 ns pulse width) is first attenuated by a variable neutral density filter (NDC-50C-4M, Thorlabs), reshaped through an iris (ID25SS, Thorlabs), and then focused by a lens. The focused beam passes through a 50 μm diameter pinhole (P50C, Thorlabs) for spatial filtering. The filtered beam is launched into a single-mode optical fiber coupler. The fiber output is collimated by a doublet (AC127-025-A, Thorlabs). The collimated beam, reflected by a two-dimensional (2D) galvanometer (6220H scanner and 673X driver, Cambridge), fills the back aperture of a doublet (AC127-025-A, Thorlabs). A compensation lens (LA1207-A, Thorlabs) is placed beneath the imaging

doublet to achieve nearly diffraction-limited optical focusing in water. A beam sampler and a fast photodiode (FDS100, Thorlabs) are inserted between the lens and pinhole to monitor the fluctuation in laser intensity. FM-OR-PAM employs a ring-shaped focused ultrasonic transducer for reflection-mode ultrasound detection. The ring transducer (35 MHz center frequency, 25 MHz bandwidth, from the Resource Center for Medical Ultrasonic Transducer Technology at the University of Southern California) has a 2 mm diameter hole in the center for the optical illumination beam to pass through and provides an acoustic focal diameter of \sim 80 μm and acoustic depth of focus of \sim 350 μm (calculated under the central frequency of the transducer). The optical and acoustic foci are aligned to maximize the detection sensitivity, and the transducer is submerged in water contained in a plastic tank for acoustic coupling. An

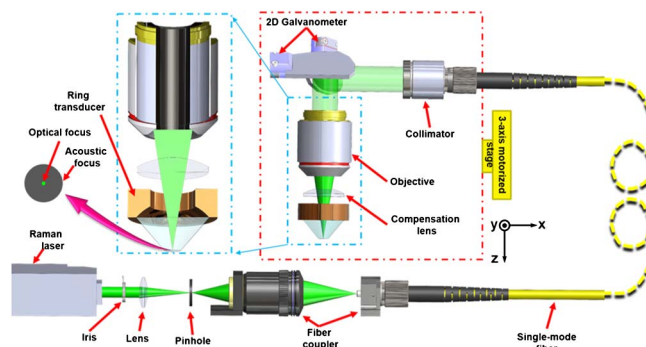


Fig. 1. Schematic of fully motorized OR-PAM.

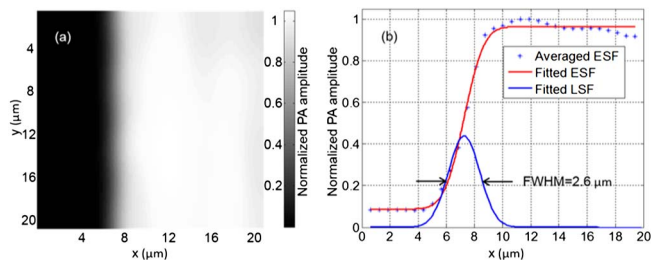


Fig. 2. Quantification of the lateral resolution of the FM-OR-PAM system. (a) Maximum-amplitude-projection (MAP) image of a sharp-edged metal square acquired with FM-OR-PAM. (b) Edge spread function (ESF) extracted from (a) and line spread function (LSF) obtained by taking the derivative of the ESF. The ESF data were averaged along y .

imaging window at the bottom of the water tank is sealed with a polyethylene membrane for optical and acoustic transmission.

FM-OR-PAM's lateral resolution (quantified in FWHM), determined by the numerical aperture of the water-immersed imaging doublet, was calculated to be $2.1 \mu\text{m}$ at 532 nm . It was experimentally quantified by imaging the sharp-edged metal square [Fig. 2(a)]. The edge-spread function (ESF) was estimated by averaging the edge of the metal square along the y axis, and was fitted to an error function ($p = A \operatorname{erf}((x - x_0)/\sigma\sqrt{2}) + B$, R^2 of 0.995) based on the assumption that the beam profile was Gaussian. The line-spread function (LSF) was then calculated as the derivative of the ESF. The lateral resolution, defined as the FWHM of the LSF, was $2.6 \mu\text{m}$ [Fig. 2(b)], which is slightly worse than the theoretical value due to the imperfect compensation of aberration.

The whole scanning head is mounted on a three-axis motorized translation stage (x and y axes, PLS-85, PI miCos GmbH; Z axis, KR15, THK. CO., LTD). The three-dimensional (3D) translation stage for mechanical scanning, in combination with the 2D galvanometer for optical scanning, provides five scanning modes: (1) 1D motion-mode (M-mode) mechanical scanning, (2) 2D mechanical scanning, (3) 3D mechanical contour scanning, (4) 2D optical scanning, and (5) synchronized 1D optical and 2D mechanical hybrid scanning.

One-dimensional M-mode mechanical scanning (mode 1) and 2D mechanical scanning (mode 2) are inherited from previously realized G2-OR-PAM as the basic functions of OR-PAM. Mode 1 was developed to measure transverse blood flow based on the photoacoustic Doppler broadening of bandwidth. In mode 1, the motor scans across the vessel of interest to acquire 2D B-scan images with a step size of $2.5 \mu\text{m}$ over $300 \mu\text{m}$ interval. At each A-line position, 200 photoacoustic A-line signals are acquired in M-mode, with a 10-kHz laser repetition rate, before the motor translates to the next position. Then the speed and direction of the transverse blood flow along the cross section can be calculated by Fourier analysis [15]. With mode 2 scanning ($2.5 \mu\text{m}$ step size in both x axis and y axis directions over a FOV of $5 \text{ mm} \times 10 \text{ mm}$), FM-OR-PAM can acquire 3D images to reveal the anatomy and hemoglobin oxygen saturation ($s\text{O}_2$) of the mouse ear vasculature with capillary-level resolution, as illustrated in Figs. 3(a) and 3(b), respectively; Fig. 3(c)

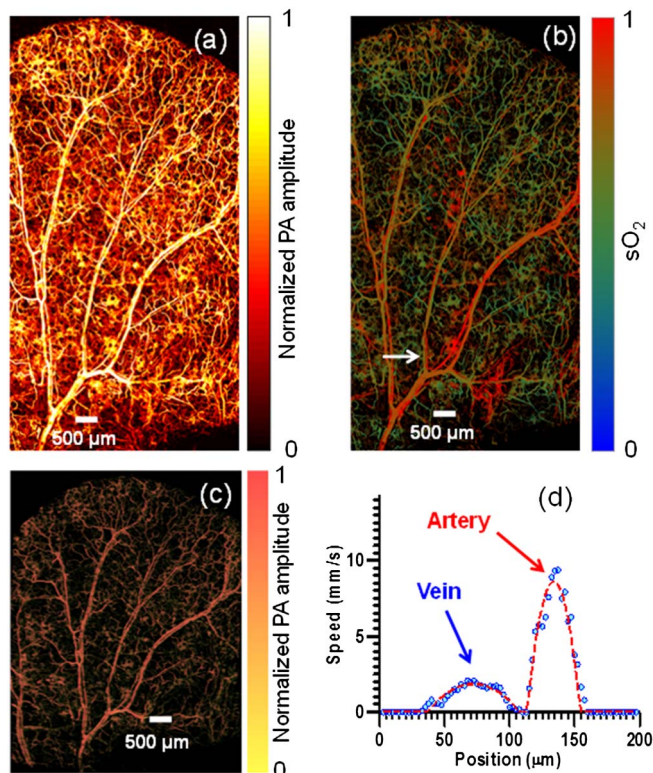


Fig. 3. *In vivo* MAP images of (a) total hemoglobin, (b) $s\text{O}_2$ (measured at 532 and 559 nm) in a mouse ear acquired with FM-OR-PAM in mode 2, and (c) 3D vasculature of the mouse ear (Media 1). (d) Blood flow distribution across the vessel pair marked with an arrow in (b) imaged in mode 1.

depicts the 3D vasculature of the whole mouse ear (Media 1). Figure 3(d) shows the blood flow measured across the selected vessel pair in mode 1. From the flow speed and $s\text{O}_2$ of the mouse ear, the metabolic rate of oxygen (MRO₂) can be calculated [16,17]. The calculated MRO₂ of this vessel pair is $0.27 \text{ ml}/100 \text{ g}/\text{min}$, which is in agreement with the data previously measured in a mouse ear [17]. The measurement of flow and $s\text{O}_2$ *in vivo* proves the capability of FM-OR-PAM for quantitative functional imaging of small animals.

To get optimal sensitivity and resolution of OR-PAM, the features of interest should be in the optical and acoustic confocal region (generally $30 \mu\text{m}$ in length in the axial direction). However, due to uneven tissue surfaces (e.g., tumors or brain), mode 2 scanning cannot capture all the features of interest within the confocal region. Here, 3D mechanical contour scanning (raster scanning with axial adjustment [18], mode 3) was integrated in FM-OR-PAM to overcome this limitation by acquiring optimally focused 3D images. The sample was first scanned in mode 2 with a coarse step size ($2.5 \mu\text{m}$ x axis motor step size, $50 \mu\text{m}$ y axis motor step size). The maximum-amplitude position in each A-line was identified to fit the set of maxima for the 2D curved surface into a coarse map. The coarse map is further linearly interpolated along the y -direction to reduce the interval to $5 \mu\text{m}$ and keeps the same x axis step size ($2.5 \mu\text{m}$). Last, the three-axis motorized translation stage scans according to the refined contour map. The acquisition time of

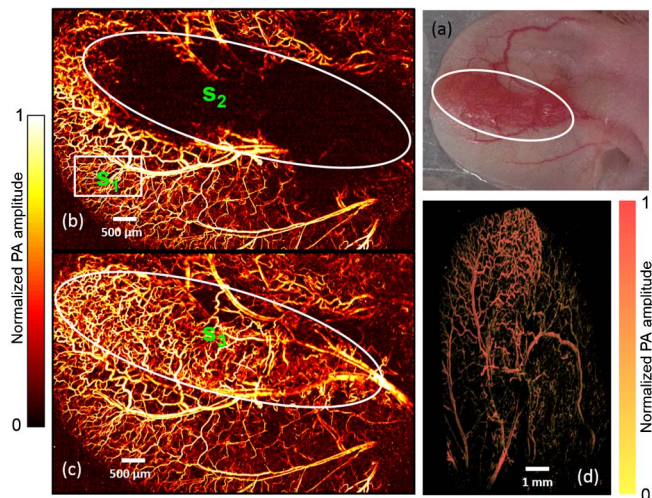


Fig. 4. Comparison of 2D mechanical scanning at one depth (mode 2) and 3D mechanical contour scanning (mode 3) of a mouse ear *in vivo*. The white circles outline the tumor region. (a) Photo of a mouse ear with a growing tumor. *In vivo* MAP images acquired with FM-OR-PAM in (b) mode 2 and (c) mode 3; (d) 3D image of the tumorous ear vasculature (Media 2).

the coarse map is about 1 min. The contour scanning can be finished in 25 minutes. Therefore, the total data acquisition time is about 26 minutes. A tumorous mouse ear with uneven surfaces [Fig. 4(a)] was imaged *in vivo* in modes 2 and 3 to prove the capability of contour scanning. The tumor region does not show up in the image acquired in mode 2 [Fig. 4(b)] due to the out-of-focus effect. Comparatively, the image acquired in mode 3 [Fig. 4(c)] reveals the vasculature of both the mouse ear and the tumor with resolved capillaries; and the 3D images [Fig. 4(d)] show the contour of the tumorous ear (Media 2). The signal to noise ratio (SNR) of the in-focus region using mode 2 scanning [s1, highlighted by white rectangle in Fig. 4(b)] is 18.1 ± 2.1 , the SNR of the tumor region [s2, highlighted by the white circle in Fig. 4(b)] is 1.5 ± 0.8 . Comparatively, the SNR of the tumor region imaged by mode 3 scanning [s3, highlighted by the white circle in Fig. 4(c)] is 15.6 ± 4.7 . We experimentally demonstrated that the mode 3 scanning can always keep the features of interest in the optical and acoustic confocal region with maintained SNR.

High-speed label-free imaging of single red blood cells (RBCs) *in vivo* with millisecond-scale temporal resolution and micrometer-scale spatial resolution holds the key to uncovering the fundamental mechanisms of cellular metabolism [19]. To this end, a voice coil-based OR-PAM system with 100 Hz B-scan rate was invented [19], and a fiber bundle-based OR-PAM system with 600 Hz B-scan rate was created [20]. Alternatively, a 2D galvanometer is employed in FM-OR-PAM to achieve high-speed optical imaging within the acoustic focus (mode 4) at a laser repetition rate of 40 kHz. *In vivo* single cell tracking is enabled by the resulting B-scan imaging over a range of 50 μm with 20 A-lines at a rate of 2 kHz or volumetric (3D) imaging over a FOV of 50 $\mu\text{m} \times 50 \mu\text{m}$ with 400 A-lines at a rate of 50 Hz. The optical scanning range was set to 50 μm , smaller than the acoustic focus, to maintain a high SNR. Figure 5(a) shows part of the ear vascular anatomy of a living nude mouse (Hsd: Athymic

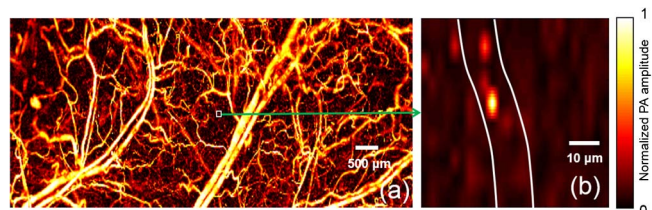


Fig. 5. *In vivo* real-time imaging of single red blood cells (RBCs) in a mouse ear. (a) MAP image acquired with FM-OR-PAM in mode 2. (b) Tracking single RBCs in a selected capillary *in vivo* in mode 4 (2D optical scanning) (Media 3).

Nude-Foxn1^{nu}, Harlan Co.), imaged in mode 2. With the site map, mode 4 is further used to monitor a small region of interest, and Fig. 5(b) shows a single RBC imaged *in vivo* in mode 4. A zoom-in sequence of RBCs flowing along the capillaries was captured in real-time video with a 20 Hz frame rate (Media 3). Mode 4 has achieved a B-scan imaging speed 20 times higher than voice-coil PAM, at the expense of FOV, which however is often not a concern if the target is cellular or capillary dynamics.

To achieve an optimal tradeoff between imaging speed and FOV, we implemented synchronized 1D optical and 2D mechanical hybrid scanning (mode 5). The scanning mechanism of mode 5 is illustrated in Fig. 6(a). In mode 5, the laser was working at a 40 kHz repetition rate. The *y* axis galvanometer repeatedly scanned with a line-scan interval of 50 μm and a line-scan rate of 2 kHz. The *x* axis motor was synchronized with the *y* axis galvanometer and moved one-step forward after the *y* axis galvanometer finished one line scan. After the *x* axis motor finished one B-scan, the *y* axis motor moved in a large step size of 50 μm (in comparison with a step size of 2.5–5.0 μm in mode 2). Figure 6(b) shows the image of a mouse ear with a 10 mm \times 8 mm FOV acquired

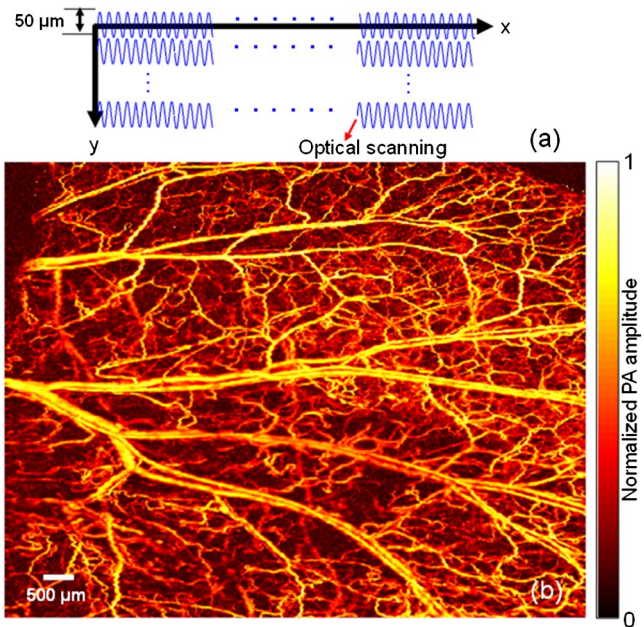


Fig. 6. Mouse ear imaging *in vivo* with FM-OR-PAM in mode 5 (synchronized 1D optical and 2D mechanical hybrid scanning). (a) Mechanism of the mode 5 scanning. (b) MAP image of the mouse ear vasculature acquired in mode 5 (Media 4).

within 150 seconds in mode 5. After mode 5 scanning, we first found the maximum amplitude (MA) point of each A-line signal. Then the MA points were rearranged following the scanning process. The rearranged MA points for each B-scan were shown in the form of animation (Media 4). With the much enlarged scanning step of the y axis motor, the imaging speed of mode 5 is 20 times faster than that of G2 OR-PAM [14].

In summary, FM-OR-PAM provides five scanning modes with high resolution, fast imaging, and a wide FOV. Its capability of tracking *in vivo* cell activities in real time and imaging uneven surfaces will be invaluable for fast and quantitative microscopic studies of tumors and the brain as long as the region of interest is optically accessible.

The authors appreciate professor James Ballard's close reading of the manuscript and thank Jinyang Liang, Chiye Li, and Yong Zhou for helpful discussions and experimental assistance. This work was sponsored in part by National Institutes of Health (NIH) grants DP1 EB016986 (NIH Director's Pioneer Award), R01 CA159959, and R01 CA134539. L.V. Wang has a financial interest in Microphotoacoustics Inc., and Endra Inc., which, however, did not support this work. K. I. Maslov has a financial interest in Microphotoacoustics Inc.

References

1. K. Maslov, H. F. Zhang, S. Hu, and L. V. Wang, *Opt. Lett.* **33**, 929 (2008).
2. L. V. Wang and S. Hu, *Science* **335**, 1458 (2012).
3. Y. Jiang, A. Forbrich, T. Harrison, and R. J. Zemp, *J. Biomed. Opt.* **17**, 036012 (2012).
4. A. Ray, J. R. Rajian, Y. E. Lee, X. Wang, and R. Kopelman, *J. Biomed. Opt.* **17**, 057004 (2012).
5. R. L. Shelton and B. E. Applegate, *Biomed. Opt. Express* **1**, 676 (2010).
6. R. L. Shelton, S. P. Mattison, and B. E. Applegate, "Volumetric imaging of erythrocytes using label-free multiphoton photoacoustic microscopy," *J. Biophotonics*, doi: 10.1002/jbio.201300059.
7. R. J. Paproski, A. E. Forbrich, K. Wachowicz, M. M. Hitt, and R. J. Zemp, *Biomed. Opt. Express* **2**, 771 (2011).
8. G. Suffredini, J. E. East, and L. M. Levy, "New applications of nanotechnology for neuroimaging," *Am. J. Neuroradiol.* (to be published).
9. S. Hu, B. Rao, K. Maslov, and L. V. Wang, *Opt. Lett.* **35**, 1 (2010).
10. S. L. Jiao, M. S. Jiang, J. M. Hu, A. Fawzi, Q. F. Zhou, K. K. Shung, C. A. Puliafito, and H. F. Zhang, *Opt. Express* **18**, 3967 (2010).
11. T. Liu, H. Li, W. Song, S. L. Jiao, and H. F. Zhang, *Curr. Eye Res.* **38**, 1229 (2013).
12. W. Song, Q. Wei, S. Jiao, and H. F. Zhang, *J. Visualized Exp.* **71**, e4390 (2013).
13. S. S. Oladipupo, S. Hu, A. C. Santeford, J. J. Yao, J. R. Kovalski, R. V. Shohet, K. Maslov, L. V. Wang, and J. M. Arbeit, *Blood* **117**, 4142 (2011).
14. S. Hu, K. Maslov, and L. V. Wang, *Opt. Lett.* **36**, 269 (2011).
15. J. J. Yao, K. I. Maslov, Y. F. Shi, L. A. Taber, and L. H. V. Wang, *Opt. Lett.* **35**, 1419 (2010).
16. S. Hu and L. V. Wang, *Front. Neuroenerg.* **2**, 10 (2010).
17. J. J. Yao, K. I. Maslov, Y. Zhang, Y. N. Xia, and L. V. Wang, *J. Biomed. Opt.* **16**, 076003 (2011).
18. H. F. Zhang, K. Maslov, M. L. Li, G. Stoica, and L. H. V. Wang, *Opt. Express* **14**, 9317 (2006).
19. L. D. Wang, K. Maslov, and L. H. V. Wang, *Proc. Natl. Acad. Sci. USA* **110**, 5759 (2013).
20. P. Hajireza, W. Shi, and R. J. Zemp, *Opt. Lett.* **36**, 4107 (2011).